
3D-GSW: 3D Gaussian Splatting Watermark for Protecting Copyrights in Radiance Fields

Youngdong Jang¹ Hyunje Park¹

Feng Yang² Heejoo Ko¹ Euijin Choo³ Sangpil Kim^{1*}

¹ Korea University ² Google Research ³ University of Alberta

Abstract

Recently, 3D Gaussian splatting has been getting a lot of attention as an innovative method for representing 3D space due to rapid rendering and image quality. However, copyright protection for the 3D Gaussian splatting has not yet been introduced. In this paper, we present a novel watermarking method for 3D Gaussian splatting. The proposed method embeds a binary message into 3D Gaussians by fine-tuning the pre-trained 3D Gaussian splatting model. To achieve this, we present Frequency-Guided Densification (FGD) that utilizes Discrete Fourier Transform to find patches with high-frequencies and split 3D Gaussians based on 3D Gaussian Contribution Vector. It is each 3D Gaussian contribution to rendered pixel colors, improving both rendering quality and bit accuracy. Furthermore, we modify an adaptive gradient mask to enhance rendering quality. Our experiments show that our method can embed a watermark in 3D Gaussians imperceptibly with increased capacity and robustness against attacks. Our method reduces optimization cost and achieves state-of-the-art performance compared to other methods.

1 Introduction

3D representation technologies have been at the center of computer vision and graphics. Such technologies play a pivotal role in various applications and industries of 3D, from movie/game production to the growing Metaverse. Since radiance field methods [10, 15, 32, 33] have shown great success in 3D representation due to their ability to achieve photo-realistic rendering with a compact implicit representation, it has been at the forefront of 3D creation.

In particular, 3D Gaussian splatting [18] (3D-GS) has emerged into the spotlight in the radiance field. 3D-GS achieves the first real-time rendering while providing high rendering quality and fast training speed. 3D-GS offers explicit representation, which uses trainable 3D Gaussians without any neural networks and directly projects 3D Gaussians onto the 2D plane, in contrast to the conventional NeRF [32]. Since this explicit property ensures that the editing capability of 3D-GS has reached unprecedented levels, 3D-GS has been a transformative method for the next generation of 3D representation.

While this is a significant advance for 3D representation, it also raises concerns about the unauthorized use of 3D content generated by the radiance field model. A straightforward approach for copyright protection is to directly embed a watermark into the content after rendering. Even if the 3D content is distorted, these watermark can be decoded. This watermarking method has a weakness. If the model is stolen, an unauthorized user can easily remove the watermark. One way to solve this drawback is

*Corresponding Author

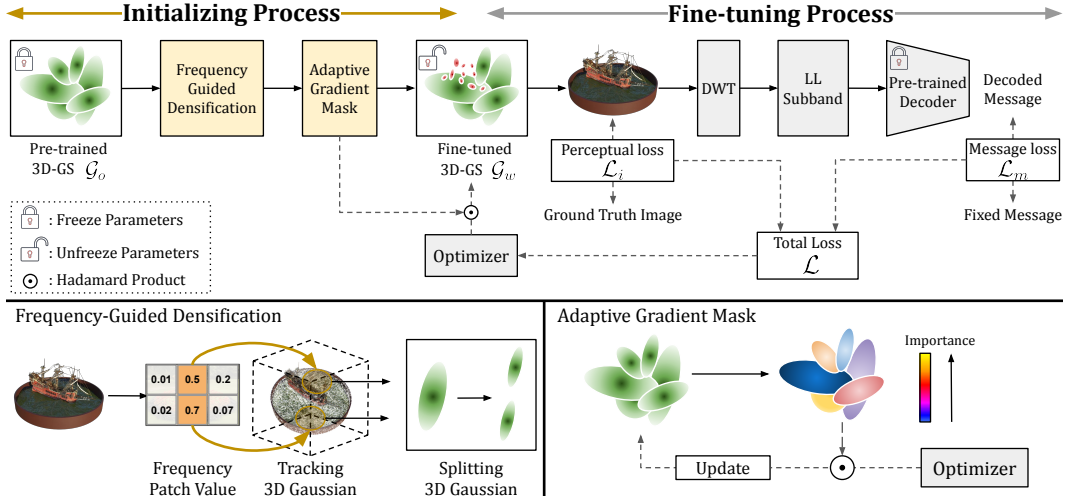


Figure 1: **3D-GSW Overview.** Before fine-tuning 3D-GS, Frequency-Guided Densification (FGD) splits 3D Gaussians into smaller and more numerous ones, and then we construct an Adaptive Gradient Mask based on the weights of a pre-trained 3D-GS \mathcal{G}_o . During the fine-tuning process, we apply the Discrete Wavelet Transform to the rendered image, and give LL subband as the input of a pre-trained HiDDeN [55] decoder. 3D-GS is optimized through the total loss \mathcal{L} , which combines perceptual loss and message loss.

to combine watermarking with the rendering process. A few studies [16, 23, 29] have been conducted to address copyright protection for the 3D content and radiance field model. However, there is no effective watermarking method for 3D-GS, although 3D-GS is the mainstream of the radiance field.

In this paper, we propose a novel watermarking method that integrates watermarks into the 3D-GS rendering process. Our method aims to invisibly embed a binary watermark message into 3D-GS. Our method fine-tunes the pre-trained 3D-GS so that the rendered images from all viewpoints hide a given message. Since this fine-tuning approach [14, 16] does not require an additional embedding process for the generated content, it can protect the copyrights of both the models and their productions. Model owners can embed a unique message into the model and provide it to different users. Even if the model is leaked, they can claim copyright on both the model and the productions used illegally.

Since capacity and invisibility are fundamental aspects in the field of watermarking, yet have a trade-off relationship, hiding and recovering a long message in the rendered image is challenging. From a capacity perspective, the more domains available for watermark embedding, the higher the capacity. From a 3D-GS perspective, small 3D Gaussians have an imperceptible effect on the rendered image quality due to minimal volume.

Motivated by these properties, we present Frequency-Guided Densification (FGD) that splits 3D Gaussians in the high-frequency area at the initialization step to make them more numerous and smaller. Since splitting all 3D Gaussians has memory limitations, we modify Error-based Densification [7], and compute 3D Gaussian Contribution Vector to find 3D Gaussians for splitting. To enhance the rendered image quality, we adopt an Adaptive Gradient Mask, which embeds a watermark into the less important 3D-GS weights, and DWT-based perceptual loss, which is focused on DWT-subbands. Furthermore, since watermarking in the frequency domain tends to be more robust than the spatial domain, we employ Discrete Wavelet Transform(DWT).

Our experiments show that our method effectively adjusts 3D Gaussians to embed the message into 3D-GS invisibly, with high capacity and robustness. We evaluate the robustness of our method under various attacks. Moreover, we compare the performance of our method with other methods [16, 29]. We show that our method outperforms the other radiance field watermarking methods across all metrics and optimizing time.

Our key contributions can be summarized as follows: (1) To the best of our knowledge, our method is the first attempt to embed a watermark into 3D-GS. (2) We propose Frequency-Guided Densification

(FGD) with 3D Gaussian Contribution Vector for achieving high capacity and invisibility. (3) We modify an Adaptive Gradient Mask and employ DWT-based perceptual loss to reduce the color artifacts while increasing capacity. (4) The proposed watermarking method achieves state-of-the-art performance, and we show that our methods are robust in various watermark attacks.

2 Related Work

2.1 3D Gaussian Splatting

Since NeRF [32] pioneers the domain of radiance fields by combining implicit neural representation and volume rendering, extensive follow-up works have aimed to either mitigate its limitation [6, 35], or explore the use of the technology [56, 21, 48, 53]. Recently, 3D Gaussian Splatting (3D-GS) [18] has brought a paradigm shift in the radiance field through a novel approach based on different branches of volume rendering. 3D-GS parametrize 3D scene with set of 3D Gaussians primitives:

$$G(\mathbf{x} : \mu, \Sigma) = e^{-\frac{1}{2}(\mathbf{x}-\mu)^T \Sigma^{-1} (\mathbf{x}-\mu)} \quad (1)$$

, where the mean μ and covariance Σ determine spatial distribution. Each 3D primitive G is projected into 2D image space primitive \hat{G} by world-to-image projective transform and its Jacobian evaluated at μ . This process is referred to as splatting. The 2D primitives are depth-ordered, rasterized, and alpha-blended using Transmittance T_i as weight to form an image:

$$I[m, n] = \sum_{i \in N_G} c_i \alpha_i T_i, \quad \text{where } T_i = \prod_{j=1}^{i-1} (1 - \alpha_j) \quad \text{and } \alpha_i = \sigma_i \hat{G}_i([m, n]; \hat{\mu}, \hat{\Sigma}) \quad (2)$$

, where c_i , σ_i and α_i are the evaluated color, opacity and density of each Gaussian primitive evaluated at each pixel. This explicit 3D representation outperforms NeRF [32] in both rendering quality and training speed while ensuring real-time rendering of scenes. Due to this performance advantage, the 3D-GS has been utilized for generative models [43, 36, 12, 25, 26] and 3D avatars [36, 40, 50].

2.2 Digital Watermarking

Frequency domain watermark. The study of embedding robust, imperceptible, and large-capacity watermarks in digital content has paralleled the evolution of digital media. The conventional 2D watermarking [5, 20, 38, 44], before the deep learning based methodology, mostly utilized domain transformation, where the watermark is embedded into selected transform coefficients. Common image transform techniques include frequency transforms, such as Discrete Fourier Transform (DFT) [49], Discrete Cosine Transform(DCT) [2, 42], and Discrete Wavelet Transform (DWT) [41].

Deep learning watermark. With advances in deep learning, watermarking methods have evolved to utilize deep learning methods [4, 27, 28, 52]. HiDDeN [55] is the first end-to-end deep watermarking methodology, introducing an approach that trains the encoder and the decoder with a noise layer between them. Subsequent studies [37, 45, 3] have utilized the frequency domain to insert more robust, invisible watermarks. With the evolution of generative models, recent watermarking research [14, 47] aims for the generative models to produce outputs, that include watermarks.

3D watermark. 3D watermarking works [46, 24, 17] have focused primarily on methods to embed and detect watermarks directly within 3D representations such as meshes and point clouds. Deep 3D-to-2D [51] shows that the watermark can be extracted when rendered with various perspectives and differentiable renderers. Since the differentiable rendering method is employed in the radiance field, watermarking for the radiance field has been considered.

2.3 Radiance Field Watermarking

StegaNeRF [23], the first approach to steganography in the radiance field, fine-tunes the pre-trained explicit radiance field model to invisibly hide image into the unimportant weight of model, using an Adaptive Gradient Mask, which is an importance-aware mask. CopyRNeRF [29] is the first end-to-end method in a digital watermarking of the radiance field. CopyRNeRF [29] explores embedding the messages into the implicit radiance field model to enhance robustness against image attacks.

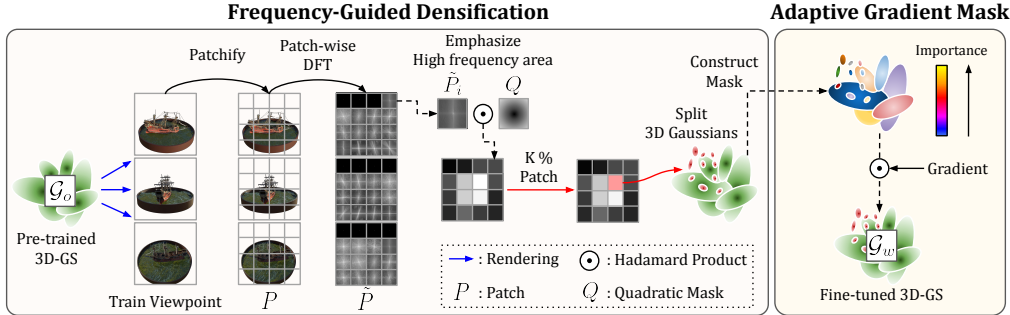


Figure 2: **Initialization process.** First, we conduct Frequency-Guided Densification (FGD). The pre-trained 3D-GS \mathcal{G}_o renders the images at all viewpoints. All rendered images are patchified and transformed into the frequency domain by using DFT. Then, we utilize a quadratic mask to emphasize high-frequency signals and split 3D Gaussians of the selected patches. Second, the importance of the weights is calculated with the split 3D-GS by Eq 9, and an Adaptive Gradient Mask is constructed by this importance. After that, 3D-GS \mathcal{G}_w is optimized with the Adaptive Gradient Mask.

WateRF [16] maintains both high image quality and robustness of watermarks through patch-wise loss, while ensuring compatibility with various NeRF representations.

However, StegaNeRF [23] is not robust against attack such as Crop, and CopyRNeRF [29] can not be applied to 3D-GS. Although WateRF [16] is applicable, it requires double rendering, resulting in long optimization times. In this paper, we present a 3D-GS watermarking method that is robust and applicable while reducing optimization time.

3 Method

We define the task of watermarking on 3D-GS as follows: Denote the pre-trained 3D-GS model as \mathcal{G}_o and watermarked model as \mathcal{G}_w . The objective is to fine-tune \mathcal{G}_o into \mathcal{G}_w by embedding a binary message $M = (m_1, \dots, m_N) \in \{0, 1\}^N$. To achieve this, we prepare the conventional decoder HiDDeN [55], denoted as D_m . We pre-train the decoder D_m in the same way as previous works [16, 14]. For invisibility and robustness, we transform the rendered image into wavelet signals, and the decoder D_m extracts M from the subband. In this section, we provide more details of each part of our method.

3.1 Overview of 3D-GSW

The conventional watermarking methods [1, 30, 55] train an encoder and a decoder to embed and extract watermarks. Unlike these methods, we do not use an encoder. If 3D-GS and the decoder are optimized simultaneously during fine-tuning, the decoder extracts the message from an image where the message is not embedded. Considering this phenomenon, we prepare the pre-trained decoder D_m , which extracts arbitrary messages. 3D-GS is fine-tuned by D_m and a fixed message M .

Before the fine-tuning, Frequency-Guided Densification (FGD) splits 3D Gaussians to ensure high capacity and rendering quality (see more details in Sec. 3.2). We also adopt an Adaptive Gradient Mask (see more details in Sec. 3.3) to more enhance rendering quality.

In the fine-tuning stage, \mathcal{G}_w renders the image $I_w \in \mathbb{R}^{H \times W \times 3}$ with the message M from diverse viewpoints. To embed more effectively, I_w is transformed into the frequency domain $W_l'^s$ by DWT:

$$W_l'^s = DWT_l(I_w) \quad (3)$$

, where $s \in \{LL, LH, HL, HH\}$ is a subband and l denotes the level of DWT. Following previous work [16], we choose the LL subband as input of D_m and decode the message $M' = D_m(W_{LL_l})$.

Message Loss. We employ a sigmoid function to confine the extracted message M' within the range of $[0, 1]$. The message loss is a Binary Cross Entropy between M and the sigmoid $sg(M')$:

$$\mathcal{L}_m = - \sum_{i=1}^N M_i \cdot \log sg(M'_i) + (1 - M_i) \cdot \log(1 - sg(M'_i)) \quad (4)$$

Perceptual Loss. The original 3D-GS \mathcal{G}_o renders the image without watermark: I_o . The perceptual loss L_i is calculated with I_w and I_o . We use LPIPS loss, \mathcal{L}_{lpips} [54] and MAE loss, \mathcal{L}_{MAE} . Since changes in DWT-subbands affect rendering quality, we design a DWT-subband loss \mathcal{L}_{DWT} to further enhance rendering quality. To utilize \mathcal{L}_{DWT} , I_o is transformed into the wavelet subbands $W_l^s = DWT_l(I_o)$. Through experiments, we find that using the LH , HL , and HH subbands improves the rendering quality during the messages recovery. By combining these losses, we construct the perceptual loss \mathcal{L}_i :

$$\mathcal{L}_{DWT} = \sum_{l,s} \mathcal{L}_{MAE}(W_l^s, W_l^s), \quad \mathcal{L}_i = \lambda_{lpips} \mathcal{L}_{lpips} + \lambda_{MAE} \mathcal{L}_{MAE} + \lambda_{DWT} \mathcal{L}_{DWT} \quad (5)$$

3D-GS are optimized in a few steps to minimize the total loss \mathcal{L} :

$$\mathcal{L} = \lambda_m \mathcal{L}_m + \mathcal{L}_i \quad (6)$$

Through this process, 3D-GS renders the images with the message embedded at every viewpoint.

3.2 Frequency-Guided Densification (FGD)

3D-GS has great power for adjusting rendered images since 3D Gaussians exist individually. Editing works [11, 13] use those advantages to edit 3D scenes by adjusting 3D Gaussians with desired constraints. In the compression works [22], 3D Gaussians are removed since they affect the rendering quality negligibly. Additionally, Human Visual System (HVS) tends to be less sensitive to variations in high-frequency signals. This property has been exploited in traditional watermarking works [9, 39].

Inspired by this, we present Frequency-Guided Densification (FGD) to split 3D Gaussians in areas with stronger high-frequency signals into smaller ones in the initialization step. First, the pre-trained 3D-GS \mathcal{G}_o renders the image I_o at all viewpoints. To manage memory usage, each image I_o is divided into patches $P \in \mathbb{R}^{U \times V}$, and each patch P_i is transformed into the frequency domain using Discrete Fourier Transform (DFT) to find the high-frequency area. After that, each transformed patch \tilde{P}_i undergoes Hadamard product \odot with a mask $Q \in \mathbb{R}^{U \times V}$, designed to emphasize high-frequency signals, and the average patch value E_i is computed

$$Q[u, v] = \left(\frac{2u - U}{U} \right)^2 + \left(\frac{2v - V}{V} \right)^2, \quad E_i = \frac{\sum_{u,v} (\tilde{P}_i \odot Q)_{uv}}{U \times V} \quad (7)$$

, where $(u, v) \in \mathbb{R}^{U \times V}$. We select the top $K\%$ patch \tilde{P} based on E_i and track 3D Gaussian belonging to the chosen patches. Motivated by Error-based densification [8], we consider 3D Gaussian Contribution Vector V_π for the rendered pixel color to choose 3D Gaussians:

$$L_\pi^{aux} := \sum_{m,n} I_\pi[m, n], \quad V_\pi := \frac{\partial L_\pi^{aux}}{\partial C'} = \alpha \hat{G} T \quad (8)$$

We compute an auxiliary loss function L_π^{aux} at a specific viewpoint π , and its derivative to get a 3D Gaussian Contribution Vector V_π . 3D Gaussians are split based on the contribution V_π , excluding those with no contribution, for memory efficiency and rendering quality. Since the number of small 3D Gaussians increases, the imperceptible domains for the message embedding become more numerous, facilitating the embedding of the message.

3.3 Adaptive Gradient Mask for 3D-GS

The purpose of watermarking is to hide data invisibly while maintaining the original quality. To achieve this, StegaNeRF [23] introduces an Adaptive Gradient Mask to embed the watermark on specific weights of the model without degrading rendering quality. Since the unimportant weights have less impact on the rendered image, the adaptive gradient mask conveys more gradients to the

unimportant weights. In StegaNeRF [23], given the pre-trained weights $\theta_0 \in \mathbb{R}^N$, the importance of weights w is calculated by $|\theta_0|^\alpha$ and a mask $z \in \mathbb{R}^N$ is constructed by w^{-1} .

In this paper, we modify the Adaptive Gradient Mask to effectively convey gradients to the unimportant weights, using the exponential function:

$$w = e^{(|\theta_0|^\alpha)}, \quad z = \frac{w^{-1}}{\sum_{i=1}^N w_i^{-1}} \quad (9)$$

, where $\alpha > 0$ adjusts the relative importance among the weights. Before fine-tuning 3D-GS, we construct mask z , based on the weight of pre-trained \mathcal{G}_o after FGD. During the fine-tuning, the gradient is masked as $\frac{\partial \mathcal{L}}{\partial \theta} \odot z$, where \mathcal{L} is Eq. 6 and \odot is a Hadamard product. The exponential function assigns smaller mask values to relatively important weights, allowing more gradients to be transmitted to less important weights. Thus, our adaptive gradient mask ensures image quality by minimizing changes in the important weights.

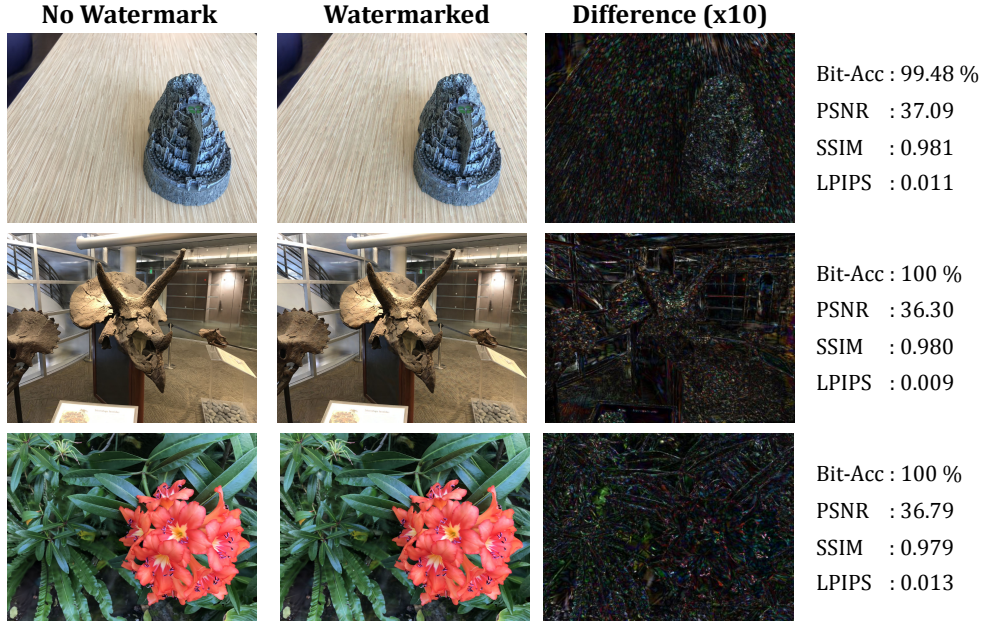


Figure 3: **The qualitative results.** It shows three types of images: No watermark, watermarked and difference (x10) between them. The results are based on 32 bits. We achieve high bit accuracy and rendering quality in LLFF dataset. As shown in the difference, our method shows embedding messages in the high-frequency domain when 3D-GS renders.

4 Experiments

4.1 Experimental Setting

Dataset & Pre-trained 3D-GS. We use Blender [32] and LLFF [31], which are considered standard in NeRF and 3D-GS [18] literature. We follow the conventional NeRF [32], wherein we compare the results using 16 scenes from the full Blender and LLFF datasets.

Baseline. To the best of our knowledge, there are no other methods suggested for watermarking in 3D-GS. Therefore, we compare our method(3D-GSW) with three strategies for fairness: 1) CopyRNeRF [29]: the first watermarking method for implicit NeRF models. 2) WateRF [16]: currently the state-of-the-art watermarking method for both implicit and explicit NeRF models. 3) WateRF [16] + 3D-GS: the original 3D-GS model with the methods in WateRF [16] applied.

Implementation Details. Our method is implemented in Pytorch [34], incorporating CUDA for the rasterization process, and trained on the single NVIDIA RTX 3090 GPU. The training is completed with epochs ranging from 2 to 10. The iteration per epoch is the number of training viewpoints in the datasets. We use Adam [19] to optimize 3D-GS. For the decoder, we pre-train HiDDeN [55] decoder for bits = {16, 32, 48} and freeze the parameters during our fine-tuning process. We set $\lambda_{lips} =$

1.2, $\lambda_{L1} = 0.6$, $\lambda_{DWT} = 0.7$, and $\lambda_m = 0.35$ in our experiments on 32 bits. Also, we use the patch size $|P| = 16$ and the top-1% frequency patches. For the adaptive gradient mask, we set $\alpha = 4$. Our experiments are conducted on five different seeds.

Evaluation. Following the settings in CopyRNeRF [29] for NeRF watermarking, we consider three important properties of watermarks: 1) **Invisibility**: We evaluate invisibility by using PSNR, SSIM, and LPIPS, which are compared between the image rendered by the fine-tuned 3D-GS and the original one. 2) **Robustness**: We investigate the effectiveness of decoding messages by measuring bit accuracy under various distortions. The following distortions for message extraction are considered: Rotation, Scaling, Gaussian blur, Crop, JPEG compression, and a combination of these distortions. 3) **Capacity**: We explore the bit accuracy across various message lengths, which are denoted as $M_b \in \{16, 32, 48\}$. Furthermore, we evaluate our method with CopyRNeRF [29], WateRF [16], and WaterRF [16] + 3D-GS on the Blender and LLFF datasets.

4.2 Experimental results

Invisibility and Capacity. Tab. 1 presents the result of rendering quality and watermark extraction performance based on the length of the message bits = {16, 32, 48}. The results show that our method increases the rendering quality with longer bits while increasing bit accuracy, compared to our baselines CopyRNeRF [29], WateRF [16] and WateRF [16]+3D-GS [18]. Although the rendering quality of WateRF [16]+3D-GS [18] is similar to ours, our method has better recovery of message bits. Therefore, our method achieves improvements in both capacity and invisibility, which have a trade-off relationship.

Fig 3 shows that our method achieves high bit accuracy, while maintaining rendering quality. Fig 4 shows that our method embeds invisible watermarks and there is less difference from the original image, compared to the baselines. Additionally, the differences in both Fig 3 and Fig 4 show that our method leads 3D-GS to embed the message into high-frequency area during rendering.

Methods	16 bits				32 bits				48 bits			
	Bit Acc↑	PSNR ↑	SSIM ↑	LPIPS ↓	Bit Acc↑	PSNR ↑	SSIM ↑	LPIPS ↓	Bit Acc↑	PSNR ↑	SSIM ↑	LPIPS ↓
CopyRNeRF [29]	91.16	26.29	0.910	0.038	78.08	26.13	0.896	0.041	60.06	27.56	0.895	0.066
WateRF [16]+NeRF [32]	94.24	28.81	0.954	0.025	86.81	27.20	0.944	0.033	70.43	28.35	0.925	0.037
WateRF [16]+TensoRF [10]	95.67	32.79	0.948	0.033	88.58	31.19	0.936	0.040	85.82	30.86	0.930	0.040
WateRF [16]+3D-GS [18]	93.43	31.00	0.961	0.053	94.94	34.87	0.978	0.048	91.50	34.37	0.976	0.051
3D-GSW (Ours)	96.96	33.00	0.971	0.019	96.70	34.89	0.982	0.012	93.00	34.52	0.980	0.009

Table 1: Bit accuracies and reconstruction qualities comparison with baselines. We show the results on 16, 32 and 48 bits. We evaluate in the same way as baselines. The results are the average of Blender and LLFF datasets. The best performances are highlighted in **bold**.

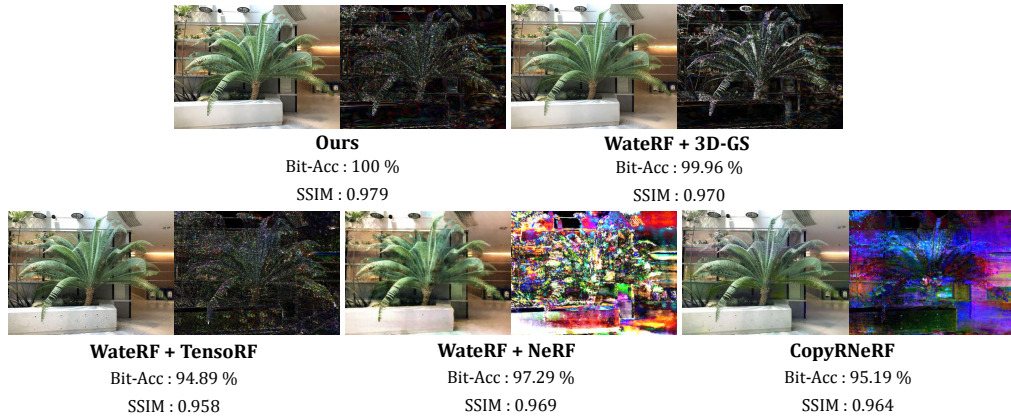


Figure 4: **Rendering quality comparison of each baseline.** 3D-GS through our method embeds the message into the high-frequency area. We show the differences ($\times 10$) between the watermarked image and the original image to each method. This results is on 32 bits.

Robustness. We assess the bit accuracy of the rendered images with the message against various attacks, including Gaussian noise, rotation, scaling, Gaussian blur, cropping, brightness adjustments,

JPEG compression, and combinations of these distortions. Tab. 2 shows that our method improves robustness against diverse attacks compared to previous works.

	No Distortion	Gaussian Noise ($v = 0.1$)	Rotation ($\pm \pi/6$)	Scaling (25%)	Gaussian Blur (deviation = 0.1)	Crop (40%)	Brightness (2.0)	JPEG Compression (10% quality)	Combined (Crop, Brightness, JPEG)
CopyRNerf [29]	91.16	90.04	88.13	89.33	90.06	-	-	-	-
WaterRF [16]+NeRF [32]	94.24	94.06	85.02	91.35	94.12	83.48	84.14	86.88	73.64
WaterRF [16]+TensoRF [10]	95.67	95.36	93.13	93.29	95.25	95.40	90.91	86.99	84.12
WaterRF [16]+3D-GS [18]	93.43	86.98	89.76	92.65	93.43	95.28	86.58	86.49	84.73
3D-GSW (Ours)	96.96	95.41	96.18	95.56	94.77	96.31	96.04	95.98	94.99

Table 2: Robustness under diverse attacks compared with the baselines. The results are the average of Blender and LLFF datasets. We show the results on $M_b = 16$ bits.

4.3 Ablation study

Impact on rendering quality. We remove each component in our methods and compare the rendering quality with the bit accuracy. Fig. 5 shows that the effect of each component in our methods. Our full method presents the best rendering quality with high bit accuracy. When each component is removed, the rendered image shows visible color differences compared to the ground truth. In other words, without all the components of our method, the invisibility of the message cannot be guaranteed. Tab. 3 shows that our full method achieves the best performance of all metrics. Thus, our method embeds the message invisibly into 3D-GS with high message extracting ability.

		Methods	Ours (3D-GSW)			
		FGD Mask L_{DWT}	Bit Acc(%) \uparrow	PSNR \uparrow	SSIM \uparrow	LPIPS \downarrow
-	-	-	96.25	28.89	0.938	0.032
✓	✓	-	95.66	29.07	0.941	0.03
✓	-	✓	95.96	28.89	0.940	0.031
-	✓	✓	95.56	30.16	0.948	0.028
✓	✓	✓	96.96	33.00	0.971	0.019

Table 3: Performance of ablation study. The results are on 16 bits.

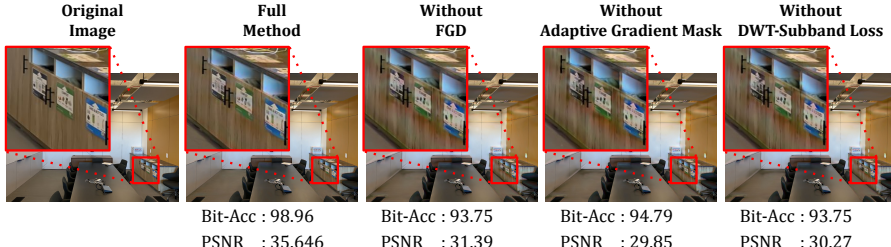


Figure 5: Reconstruction quality comparisons. We evaluate our full method, our method without FGD, Adaptive Gradient Mask and without DWT-Subband loss on 16 bits.

Effect of Frequency Guided Densification. In this section, we present the impact of Frequency Guided Densification (FGD) on rendered images of 3D-GS before fine-tuning. FGD makes 3D Gaussians in the high-frequency areas smaller and more numerous to ensure that there is no perceptible change in rendering quality to the human eyes. Fig. 6 shows that FGD successfully adjusted 3D Gaussians in the area of the image with high-frequencies. Therefore, we identify domains capable of accommodating a large number of inserted bits, and show the preservation of rendering quality.

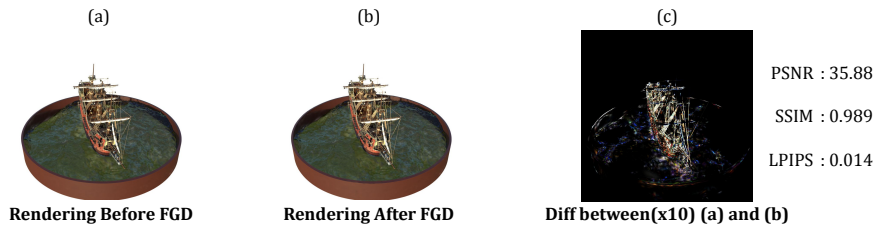


Figure 6: Comparison of FGD effect on the rendered image. Through FGD, we achieve adding 3D Gaussians into high-frequency areas without degrading rendering quality.

Effect of 3D Gaussian Contribution Vector. During Frequency-Guided Densification (FGD), we compute the contribution v_k of each 3D Gaussian to the rendered image. FGD tracks 3D Gaussians

based on their contribution to the pixels and splits only Gaussians with $v_k \neq 0$. In other words, it does not split 3D Gaussians without the contribution, i.e. $v_k = 0$. In our experiment, we show the high reliability of our computed Gaussian contributions.



Figure 7: Rendered image by contribution. We selected 3D Gaussians based on their contribution v_k , and rendered them with pre-trained 3D-GS. Since the difference(x10) between (a) and (b) is zero, v_k expresses the contribution of each 3D Gaussian effectively.

DWT subband loss. Increasing the performance of both bit accuracy and rendering quality is challenging. To address this challenge, we design DWT-subband loss to improve rendering quality, while increasing bit accuracy. Since DWT transforms an image into diverse subbands, $\{LL, LH, HL, HH\}$, the perceptual loss can be calculated by using the signal of the original image and the watermarked image. We use $\{LH, HL, HH\}$ subbands as inputs of L_{MAE} loss and add these L_{MAE} losses to improve both the bit accuracy and the rendering quality. In this experiment, the performance is compared by adding LL subband to our DWT-subband loss. Tab. 4 shows that the best way is for LH, HL, and HH to increase without degrading bit accuracy.

Comparison of optimizing time. Previous work, CopyRNerf [29], uses the implicit NeRF [32], which requires significant optimizing time. To solve this problem, WateRF [16] presents a fast optimizing method. However, when WateRF [16] is applied to 3D-GS which requires a lot of memory, the cost is increased due to twice rendering in one iteration. Thus, our method, 3D-GSW, aims to reduce the optimizing cost and time to embed messages into 3D-GS, rendering only once in a single iteration. Fig. 8 shows that our method quickly converges to high bit accuracy, compared to previous methods. As a result, we achieve faster optimization time than previous methods.

5 Limitations and Future Work

Limitations. Since our proposed method requires the pre-trained decoder, the decoder pre-training must be done first. Fortunately, the decoder only needs to be trained once per length of bits, and after training, the pre-training process for the corresponding length is not required. Additionally, due to the substantial memory requirements of 3D-GS, there are inherent limitations on the extent to which the number of 3D Gaussians can be increased. Today, 3D-GS is the mainstream of the radiance field due to high rendering quality and fast training speed. However, if 3D-GS were to lose popularity, the expansion of the proposed method would be limited.

Future Work. For future work, there is value in training 3D-GS and the decoder together end-to-end, as compression studies for 3D-GS are actively underway. Another direction is improving the decoder to be more robust against various distortions. Furthermore, research on embedding watermarks into models combining 3D-GS and generative models is also valuable.

Subband	Bit Acc↑	PSNR ↑	SSIM ↑	LPIPS ↓
LL, LH, HL, HH	92.48	34.82	0.976	0.0405
LH, HL, HH	96.70	34.89	0.982	0.012

Table 4: **DWT subband loss.** The results are the average of Blender and LLFF datasets. We show the results on 32 bits.

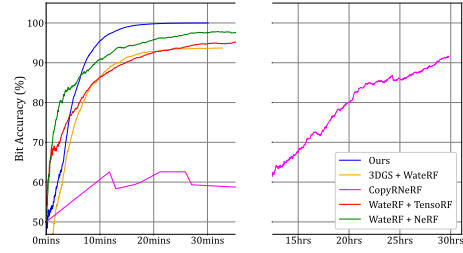


Figure 8: Training time for the Blender dataset experiment. Our method increases bit accuracy faster than other methods.

6 Conclusion

We present the first watermarking method for 3D Gaussian Splatting by developing a novel densification method, Frequency-Guided Densification (FGD). FGD searches for patches with high-frequency in the rendered image, making the 3D Gaussians corresponding to those regions smaller and more numerous. As a result, it ensures high capacity and rendering quality. Additionally, we adopt 3D Gaussians Contribution Vector to manage memory usage. To enhance rendering quality while maintaining high bit accuracy, we modify the Adaptive Gradient Masking strategy and introduce DWT-subband loss. Our experiments show that our method ensures high capacity, embeds invisible watermarks, and guarantees robustness. Additionally, compared to previous methods, we reduce the optimization cost and achieve state-of-the-art performance.

References

- [1] Mahdi Ahmadi, Alireza Norouzi, Nader Karimi, Shadrokh Samavi, and Ali Emami. Redmark: Framework for residual diffusion watermarking based on deep networks. *Expert Systems with Applications*, 146:113157, 2020.
- [2] Nasir Ahmed, T. Natarajan, and Kamisetty R Rao. Discrete cosine transform. *IEEE transactions on Computers*, 100(1):90–93, 1974.
- [3] C Annadurai, I Nelson, K Nirmala Devi, R Manikandan, and Amir H Gandomi. Image watermarking based data hiding by discrete wavelet transform quantization model with convolutional generative adversarial architectures. *Applied Sciences*, 13(2):804, 2023.
- [4] Shumeet Baluja. Hiding images in plain sight: Deep steganography. *Advances in neural information processing systems*, 30, 2017.
- [5] Mauro Barni, Franco Bartolini, and Alessandro Piva. Improved wavelet-based watermarking through pixel-wise masking. *IEEE transactions on image processing*, 10(5):783–791, 2001.
- [6] Wenjing Bian, Zirui Wang, Kejie Li, Jia-Wang Bian, and Victor Adrian Prisacariu. Nope-nerf: Optimising neural radiance field with no pose prior. In *Proceedings of the IEEE/CVF Conference on Computer Vision and Pattern Recognition*, pages 4160–4169, 2023.
- [7] Samuel Rota Bulò, Lorenzo Porzi, and Peter Kortschieder. Revising densification in gaussian splatting. *arXiv preprint arXiv:2404.06109*, 2024.
- [8] Samuel Rota Bulò, Lorenzo Porzi, and Peter Kortschieder. Revising densification in gaussian splatting, 2024.
- [9] Patrizio Campisi, Alessandro Neri, and Marco Visconti. Wavelet-based method for high-frequency subband watermark embedding. In *Multimedia Systems and Applications III*, volume 4209, pages 344–353. SPIE, 2001.
- [10] Anpei Chen, Zexiang Xu, Andreas Geiger, Jingyi Yu, and Hao Su. Tensorf: Tensorial radiance fields. In *European Conference on Computer Vision*, pages 333–350. Springer, 2022.
- [11] Yiwen Chen, Zilong Chen, Chi Zhang, Feng Wang, Xiaofeng Yang, Yikai Wang, Zhongang Cai, Lei Yang, Huaping Liu, and Guosheng Lin. Gaussianeditor: Swift and controllable 3d editing with gaussian splatting. *arXiv preprint arXiv:2311.14521*, 2023.
- [12] Zilong Chen, Feng Wang, and Huaping Liu. Text-to-3d using gaussian splatting. *arXiv preprint arXiv:2309.16585*, 2023.
- [13] Jiemin Fang, Junjie Wang, Xiaopeng Zhang, Lingxi Xie, and Qi Tian. Gaussianeditor: Editing 3d gaussians delicately with text instructions. *arXiv preprint arXiv:2311.16037*, 2023.
- [14] Pierre Fernandez, Guillaume Couairon, Hervé Jégou, Matthijs Douze, and Teddy Furon. The stable signature: Rooting watermarks in latent diffusion models. In *Proceedings of the IEEE/CVF International Conference on Computer Vision*, pages 22466–22477, 2023.

[15] Sara Fridovich-Keil, Alex Yu, Matthew Tancik, Qinhong Chen, Benjamin Recht, and Angjoo Kanazawa. Plenoxels: Radiance fields without neural networks. In *Proceedings of the IEEE/CVF Conference on Computer Vision and Pattern Recognition*, pages 5501–5510, 2022.

[16] Youngdong Jang, Dong In Lee, MinHyuk Jang, Jong Wook Kim, Feng Yang, and Sangpil Kim. Waterf: Robust watermarks in radiance fields for protection of copyrights, 2024.

[17] Imen Fourati Kallel, Ahmed Grati, and Amina Taktak. 3d data security: Robust 3d mesh watermarking approach for copyright protection. In *Examining Multimedia Forensics and Content Integrity*, pages 1–37. IGI Global, 2023.

[18] Bernhard Kerbl, Georgios Kopanas, Thomas Leimkühler, and George Drettakis. 3d gaussian splatting for real-time radiance field rendering. *ACM Transactions on Graphics*, 42(4):1–14, 2023.

[19] Diederik P Kingma and Jimmy Ba. Adam: A method for stochastic optimization. *arXiv preprint arXiv:1412.6980*, 2014.

[20] Martin Kutter, Frederic D Jordan, and Frank Bossen. Digital signature of color images using amplitude modulation. In *Storage and Retrieval for Image and Video Databases V*, volume 3022, pages 518–526. SPIE, 1997.

[21] Ke Lan. Dream fusion in octahedral spherical hohlraum. *Matter and Radiation at Extremes*, 7(5), 2022.

[22] Joo Chan Lee, Daniel Rho, Xiangyu Sun, Jong Hwan Ko, and Eunbyung Park. Compact 3d gaussian representation for radiance field. *arXiv preprint arXiv:2311.13681*, 2023.

[23] Chenxin Li, Brandon Y Feng, Zhiwen Fan, Panwang Pan, and Zhangyang Wang. Steganerf: Embedding invisible information within neural radiance fields. In *Proceedings of the IEEE/CVF International Conference on Computer Vision*, pages 441–453, 2023.

[24] De Li, Zhenren Yang, and Xun Jin. Zero watermarking scheme for 3d triangle mesh model based on global and local geometric features. *Multimedia Tools and Applications*, 82(28):43635–43648, 2023.

[25] Yixun Liang, Xin Yang, Jiantao Lin, Haodong Li, Xiaogang Xu, and Yingcong Chen. Lucid-dreamer: Towards high-fidelity text-to-3d generation via interval score matching. *arXiv preprint arXiv:2311.11284*, 2023.

[26] Huan Ling, Seung Wook Kim, Antonio Torralba, Sanja Fidler, and Karsten Kreis. Align your gaussians: Text-to-4d with dynamic 3d gaussians and composed diffusion models. *arXiv preprint arXiv:2312.13763*, 2023.

[27] Xiyang Luo, Yinxiao Li, Huiwen Chang, Ce Liu, Peyman Milanfar, and Feng Yang. Dvmark: a deep multiscale framework for video watermarking. *IEEE Transactions on Image Processing*, 2023.

[28] Xiyang Luo, Ruohan Zhan, Huiwen Chang, Feng Yang, and Peyman Milanfar. Distortion agnostic deep watermarking. In *Proceedings of the IEEE/CVF conference on computer vision and pattern recognition*, pages 13548–13557, 2020.

[29] Ziyuan Luo, Qing Guo, Ka Chun Cheung, Simon See, and Renjie Wan. Copyrnerf: Protecting the copyright of neural radiance fields. In *Proceedings of the IEEE/CVF International Conference on Computer Vision*, pages 22401–22411, 2023.

[30] Debolina Mahapatra, Preetam Amrit, Om Prakash Singh, Amit Kumar Singh, and Amrit Kumar Agrawal. Autoencoder-convolutional neural network-based embedding and extraction model for image watermarking. *Journal of Electronic Imaging*, 32(2):021604–021604, 2023.

[31] Ben Mildenhall, Pratul P Srinivasan, Rodrigo Ortiz-Cayon, Nima Khademi Kalantari, Ravi Ramamoorthi, Ren Ng, and Abhishek Kar. Local light field fusion: Practical view synthesis with prescriptive sampling guidelines. *ACM Transactions on Graphics (TOG)*, 38(4):1–14, 2019.

[32] Ben Mildenhall, Pratul P Srinivasan, Matthew Tancik, Jonathan T Barron, Ravi Ramamoorthi, and Ren Ng. Nerf: Representing scenes as neural radiance fields for view synthesis. *Communications of the ACM*, 65(1):99–106, 2021.

[33] Thomas Müller, Alex Evans, Christoph Schied, and Alexander Keller. Instant neural graphics primitives with a multiresolution hash encoding. *ACM transactions on graphics (TOG)*, 41(4):1–15, 2022.

[34] Adam Paszke, Sam Gross, Francisco Massa, Adam Lerer, James Bradbury, Gregory Chanan, Trevor Killeen, Zeming Lin, Natalia Gimelshein, Luca Antiga, et al. Pytorch: An imperative style, high-performance deep learning library. *Advances in neural information processing systems*, 32, 2019.

[35] Albert Pumarola, Enric Corona, Gerard Pons-Moll, and Francesc Moreno-Noguer. D-nerf: Neural radiance fields for dynamic scenes. In *Proceedings of the IEEE/CVF Conference on Computer Vision and Pattern Recognition*, pages 10318–10327, 2021.

[36] Zhiyin Qian, Shaofei Wang, Marko Mihajlovic, Andreas Geiger, and Siyu Tang. 3dgs-avatar: Animatable avatars via deformable 3d gaussian splatting. *arXiv preprint arXiv:2312.09228*, 2023.

[37] R Radha Kumari, V Vijaya Kumar, and K Rama Naidu. Deep learning-based image watermarking technique with hybrid dwt-svd. *The Imaging Science Journal*, pages 1–17, 2023.

[38] MS Raval and PP Rege. Discrete wavelet transform based multiple watermarking scheme. In *TENCON 2003. Conference on Convergent Technologies for Asia-Pacific Region*, volume 3, pages 935–938. IEEE, 2003.

[39] Praful Saxena, Shanon Garg, and Arpita Srivastava. Dwt-svd semi-blind image watermarking using high frequency band. In *2nd International Conference on Computer Science and Information Technology (ICCSIT)*, pages 28–29. Citeseer, 2012.

[40] Zhijing Shao, Zhaolong Wang, Zhuang Li, Duotun Wang, Xiangru Lin, Yu Zhang, Mingming Fan, and Zeyu Wang. Splattingavatar: Realistic real-time human avatars with mesh-embedded gaussian splatting. *arXiv preprint arXiv:2403.05087*, 2024.

[41] Mark J Shensa et al. The discrete wavelet transform: wedding the a trous and mallat algorithms. *IEEE Transactions on signal processing*, 40(10):2464–2482, 1992.

[42] Gilbert Strang. The discrete cosine transform. *SIAM review*, 41(1):135–147, 1999.

[43] Jiaxiang Tang, Jiawei Ren, Hang Zhou, Ziwei Liu, and Gang Zeng. Dreamgaussian: Generative gaussian splatting for efficient 3d content creation. *arXiv preprint arXiv:2309.16653*, 2023.

[44] Peining Tao and Ahmet M Eskicioglu. A robust multiple watermarking scheme in the discrete wavelet transform domain. In *Internet Multimedia Management Systems V*, volume 5601, pages 133–144. SPIE, 2004.

[45] Alireza Tavakoli, Zahra Honjani, and Hedieh Sajedi. Convolutional neural network-based image watermarking using discrete wavelet transform. *International Journal of Information Technology*, 15(4):2021–2029, 2023.

[46] Bianca Jansen van Rensburg, Pauline Puteaux, William Puech, and Jean-Pierre Pedeboy. 3d object watermarking from data hiding in the homomorphic encrypted domain. *ACM Transactions on Multimedia Computing, Communications and Applications*, 19(5s):1–20, 2023.

[47] Yuxin Wen, John Kirchenbauer, Jonas Geiping, and Tom Goldstein. Tree-rings watermarks: Invisible fingerprints for diffusion images. *Advances in Neural Information Processing Systems*, 36, 2024.

[48] Chung-Yi Weng, Brian Curless, Pratul P Srinivasan, Jonathan T Barron, and Ira Kemelmacher-Shlizerman. Humannerf: Free-viewpoint rendering of moving people from monocular video. In *Proceedings of the IEEE/CVF conference on computer vision and pattern Recognition*, pages 16210–16220, 2022.

- [49] Shmuel Winograd. On computing the discrete fourier transform. *Mathematics of computation*, 32(141):175–199, 1978.
- [50] Yuelang Xu, Benwang Chen, Zhe Li, Hongwen Zhang, Lizhen Wang, Zerong Zheng, and Yebin Liu. Gaussian head avatar: Ultra high-fidelity head avatar via dynamic gaussians. *arXiv preprint arXiv:2312.03029*, 2023.
- [51] Innfarm Yoo, Huiwen Chang, Xiyang Luo, Ondrej Stava, Ce Liu, Peyman Milanfar, and Feng Yang. Deep 3d-to-2d watermarking: Embedding messages in 3d meshes and extracting them from 2d renderings. In *Proceedings of the IEEE/CVF Conference on Computer Vision and Pattern Recognition*, pages 10031–10040, 2022.
- [52] Chaoning Zhang, Philipp Benz, Adil Karjauv, Geng Sun, and In So Kweon. Udh: Universal deep hiding for steganography, watermarking, and light field messaging. *Advances in Neural Information Processing Systems*, 33:10223–10234, 2020.
- [53] Jingbo Zhang, Xiaoyu Li, Ziyu Wan, Can Wang, and Jing Liao. Text2nerf: Text-driven 3d scene generation with neural radiance fields. *IEEE Transactions on Visualization and Computer Graphics*, 2024.
- [54] Richard Zhang, Phillip Isola, Alexei A Efros, Eli Shechtman, and Oliver Wang. The unreasonable effectiveness of deep features as a perceptual metric. In *CVPR*, 2018.
- [55] Jiren Zhu, Russell Kaplan, Justin Johnson, and Li Fei-Fei. Hidden: Hiding data with deep networks. In *Proceedings of the European conference on computer vision (ECCV)*, pages 657–672, 2018.
- [56] Zihan Zhu, Songyou Peng, Viktor Larsson, Weiwei Xu, Hujun Bao, Zhaopeng Cui, Martin R Oswald, and Marc Pollefeys. Nice-slam: Neural implicit scalable encoding for slam. In *Proceedings of the IEEE/CVF Conference on Computer Vision and Pattern Recognition*, pages 12786–12796, 2022.